J Mater Sci: Mater Electron (2018) 29:906–913
DOI 10.1007/s10854-017-7987-y

Structural and optical characterization of RE (Eu^{2+}, Ce^{3+}) doped $SrMg_2Al_6Si_9O_{30}$ nanocrystalline phosphor

M. M. Kolte[1] · V. B. Pawade[2] · S. J. Dhoble[1]

Received: 4 August 2017 / Accepted: 3 October 2017 / Published online: 13 October 2017

Abstract This article present the reports on optical study of Eu^{2+} and Ce^{3+} doped $SrMg_2Al_6Si_9O_{30}$ phosphors, which has been synthesized by combustion method at 550 °C. Here $SrMg_2Al_6Si_9O_{30}$:Eu^{2+} emission band observed at 425 nm by keeping the excitation wavelength constant at 342 nm, whereas $SrMg_2Al_6Si_9O_{30}$:Ce^{3+} ions shows the broad emission band at 383 nm, under 321 nm excitation wavelength, both the emission bands are assigned due to 5d–4f transition respectively. Further, phase purity, morphology and crystallite size are confirmed by XRD, SEM and TEM analysis. However, the TGA analysis is carried out to know the amount of weight lost during the thermal processing. The CIE coordinates of $SrMg_2Al_6Si_9O_{30}$:Eu^{2+} phosphor is observed at x = 0.160, y = 0.102 respectively, which may be used as a blue component for NUV-WLEDs. The critical distance of energy transfer between Ce^{3+} ions and host lattice is found to be 10.65 Å.

1 Introduction

Today, the whole world facing an problem associated with energy conservation and consumption reduction. Advanced materials is an emerging fields to solve the problem deals with energy by using a novel materials having the energy saving potential and storage capabilities. Thus, in case of applied as well as basic research fields, recently rare earth doped oxides based phosphor materials received an fast-growing interest due to their merits in high luminous efficiency, energy savings, potential, environmental friendliness, long persistence and reliability, high thermal and chemical stability [1, 2]. Among the different host used in luminescent materials aluminosilicates is an best candidates due to their physical, chemical properties and stability. There are very few work has been done on rare earth activated aluminosilicates host phosphors, because they have required high temperature for the phase formation due the combination of tetrahedral Al^{3+} and Si^{4+} bonding in their crystal structure. Also the mechanism of energy transfer between two different emission centres plays an important role in the development of luminescent display devices due to their theoretical and practical applications [3]. The luminescence efficiency of various rare earth ions can be enhanced by the energy transfer process from other co-doped rare earth ions; because most of the rare earth ions, have only narrow f–f transition lines from 300 to 500 nm locate at the range of near-UV, have low oscillator strength. Therefore rare earth ions have limitations in the application of UV–LED phosphors. Thus to avoid this drawback, RE ions with broad band emitting ions, such as Ce^{3+}, Eu^{2+} can be co-doped as sensitizers and it help in improving the luminescence properties of the phosphors materials [4–7]. There are some well known reported aluminosilicates based phosphor such as, $BaMg_2Al_6Si_9O_{30}$:Eu^{2+} [8], $NaAlSiO_4$:Dy^{3+} [9], $Sr_3Al_8SiO_{17}$:Eu^{2+} [10]. Wei Lu et al. had reported $SrMg_2Al_6Si_9O_{30}$:Eu^{2+}, Mn^{2+} phosphor synthesized by solid state reaction method [11]. In the present work we have reported optical properties of Eu^{2+} and Ce^{3+} doped $SrMg_2Al_6Si_9O_{30}$:phosphors, which has been synthesized here by combustion method successfully.

✉ V. B. Pawade
vijaypawade003@gmail.com

[1] Department of Physics, R.T.M. Nagpur University, Nagpur 440033, India

[2] Department of Applied-Physics, Laxminarayan Institute of Technology, R.T.M. Nagpur University, Nagpur 440033, India

2 Materials and methods

A series RE (RE = Eu^{2+}, Ce^{3+}) doped $SrMg_2Al_6Si_9O_{30}$ were synthesized via combustion synthesis route at 550 °C. The precursors used for the synthesis of $SrMg_2Al_6Si_9O_{30}$:Eu^{2+} and $SrMg_2Al_6Si_9O_{30}$:Ce^{3+} phosphors were analytical grade $SrNO_3$, $Mg(NO_3)_2$, $Al(NO_3)_3{\cdot}9H_2O$, SiO_2(A.R.), NH_2CONH_2, $(NH_4)_2Ce(NO_3)_6$, Eu_2O_3. Here, metal nitrates were used as oxidizers, and urea (NH_2CONH_2) was used as fuel for combustion. Using the concept of propellant chemistry, the weight of all the ingredients used above were calculated and ground together in mortal pestle to the form a pasty solution. While crushing, to make the solution more homogeneous, small amount of dilute nitric acid was added to the mixture. After mixing for about 15 min, pasty solution was transferred to the china dish and the dish was then inserted into a vertical muffle furnace preheated at 550 °C. Within 3–5 min, the exothermic reaction between metal nitrates and organic fuel complexes at low temperature takes place resulting into the formation of a flame and then highly fluffy and porous crystalline material is formed which after crushing becomes ready for the characterization. Initially the prepared phosphor is well characterized by using X-ray diffraction techniques to confirm the phase purity of the phosphor. This study was carried out at room temperature using a PAN-analytical diffractometer with Cu-K_α radiation (1.5405 Å) under operating voltage at 40 kV and current 30 mA respectively having the scan step time at 10.3377 s in a wide range of Bragg angle $10° < 2\theta < 80°$. The photoluminescence emission and excitation spectra were recorded using Shimadzu make RF5301PC spectrofluorometer using solid sample holder. The measurement were done by taking the same amount of sample at room temperature. The surface morphology of the sample is observed with the help of scanning electron microscopy (SEM), JEOL-6380 A under the sub micrometer resolution. The crystallites size of the phosphor particles has been studies with the help of Transmission electron microscopy (TEM) at an 200 keV accelerating voltage. Thermal analysis of the sample is studies by using TGA, to know the amount of weight loss during the thermal processing the sample using Hitachi STA7200 thermal analyser on accurately weighed $SrMg_2Al_6Si_9O_{30}$ sample (about 10.37 mg) in suitable air atmosphere by heating from 40 to 900 °C at a heating rate of 10 °C/min.

3 Results and discussion

The prepared phosphor was characterized by using the following techniques at standard measurement.

3.1 X-ray diffraction

Figure 1 shows, the XRD pattern of $SrMg_2Al_6Si_9O_{30}$ phosphor by combustion synthesis technique which has not been reported elsewhere. All of the diffraction peaks are in good agreement with the standard JPCDS file no. 83-0741 [12]. Besides that there are some unwanted impurity peaks seen in diffraction pattern which may observed due to addition of atmospheric impurity during synthesis process. But from the single most intense peak in the diffraction pattern, we can conclude that the synthesized phosphor compound has the single phase. The peaks are broadened which indicates the nanocrystallinity of the $SrMg_2Al_6Si_9O_{30}$ sample. $SrMg_2Al_6Si_9O_{30}$ crystallizes in hexagonal unit cell with space group P6/mcc and being reported lattice parameters as a = b = 10.1273 Å, c = 14.2274 Å, $\alpha = \beta = 90°$, $\gamma = 120°$. The cell volume (V) = 1263.70 $Å^3$ and the number of molecules in the unit cell (Z) = 2. Figure 2a gives schematic representation of crystal structure of $SrMg_2Al_6Si_9O_{30}$ phosphor. As shown in the Fig. 2b, c $SrMg_2Al_6Si_9O_{30}$ provide 12-fold coordinated Sr^{2+} site and sixfold coordinated Mg^{2+} cation site for appropriate.

3.2 Surface morphology

The visual image of the nano particles of $SrMg_2Al_6Si_9O_{30}$:Ce^{3+}were analyzed by SEM micrographs as shown in Fig. 3. SEM micrographs and particle size investigation of the phosphor shows that crystallinity, particle size, and surface roughness of the phosphor materials shows noticeable effect on the PL intensity. It depicts the thin plate with laminar structure. First micrograph shows a fibrous microstructure with filter paper like morphology [13, 14] with voids, pores and cracks. The particles sizes are revealing slight larger than that from the XRD data as SEM shows

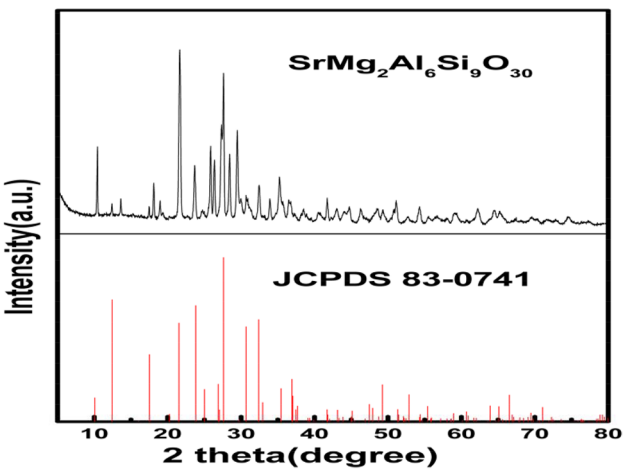

Fig. 1 X-ray diffraction pattern of $SrMg_2Al_6Si_9O_{30}$ phosphor

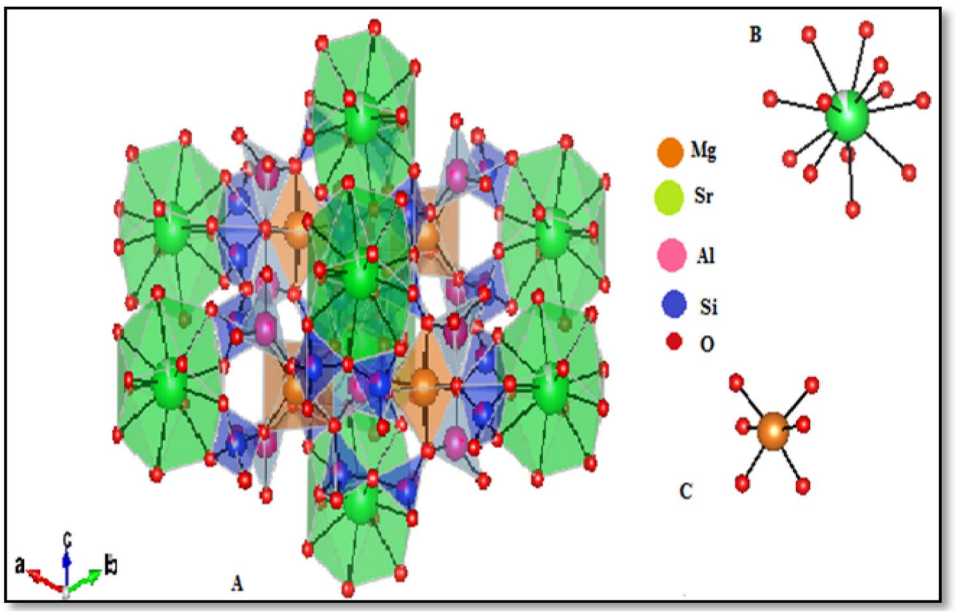

Fig. 2 **a** Schematic representation of crystal structure of $SrMg_2Al_6Si_9O_{30}$ phosphor, however **b** and **c** represent the Sr^{2+} (12 coordinated) and Mg^{2+} (6-coordinated) cation sites in the host lattice

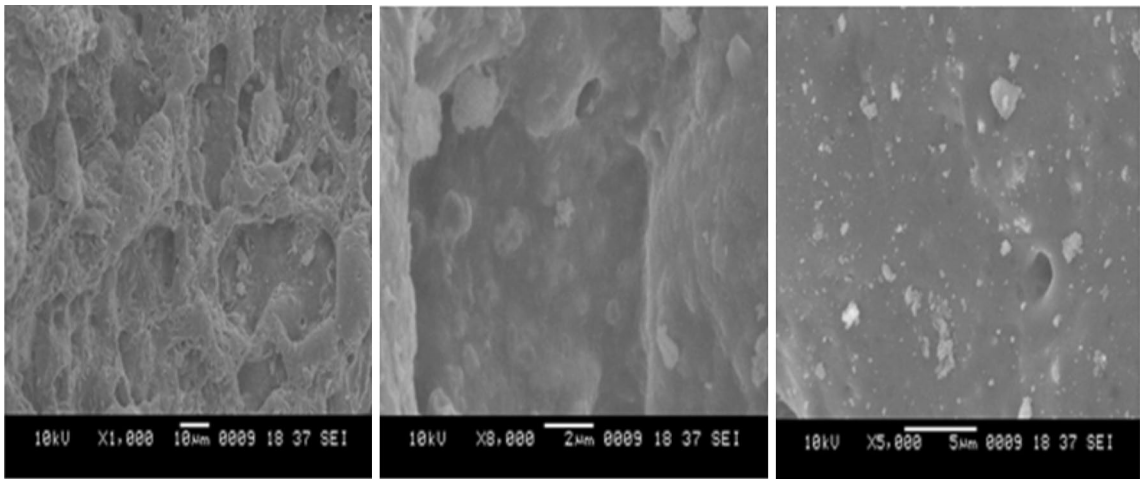

Fig. 3 SEM images of $SrMg_2Al_6Si_9O_{30}$ phosphor

the lateral dimension of the particles while XRD gives the regularity in the atomic arrangement. Lateral dimension of the particles is of the order of a few micrometers, on the other hand the individual nanoparticle with regular atomic lattice varies up to a few nanometers. The smooth surface of phosphor can reduce the non-radiation and scattering, hence is beneficial to the luminescence efficiency in application. The dense packed arrangement of small particles can avert the phosphors from aging. The SEM micrographs in Fig. 3 also show some agglomeration of interlinked particles. The combustion reaction produces substantial moles of gas for each mole of solid produce. The rapid evolution of these gases break up large agglomerates and yield a porous nature phosphor powder that occupies the volume of the reaction crucible. The surface area to volume ratio of the combustion-synthesized powder is usually very large due to the large porosity between individual particles, which has appeared in the SEM micrographs [15].

3.3 Crystallites size

Transmission electron microscopy (TEM) is a useful technique in determining crystal morphology and particle size of materials. It is difficult to measure the actual grain size distribution due to agglomeration and low magnification of present SEM micrographs hence the TEM analysis of the phosphor has been carried out and the obtained results are presented below. The transmission electron micrograph (TEM) of $SrMg_2Al_6Si_9O_{30}$ were shown in Fig. 4. From the micrographs, the average crystallite size was observed to

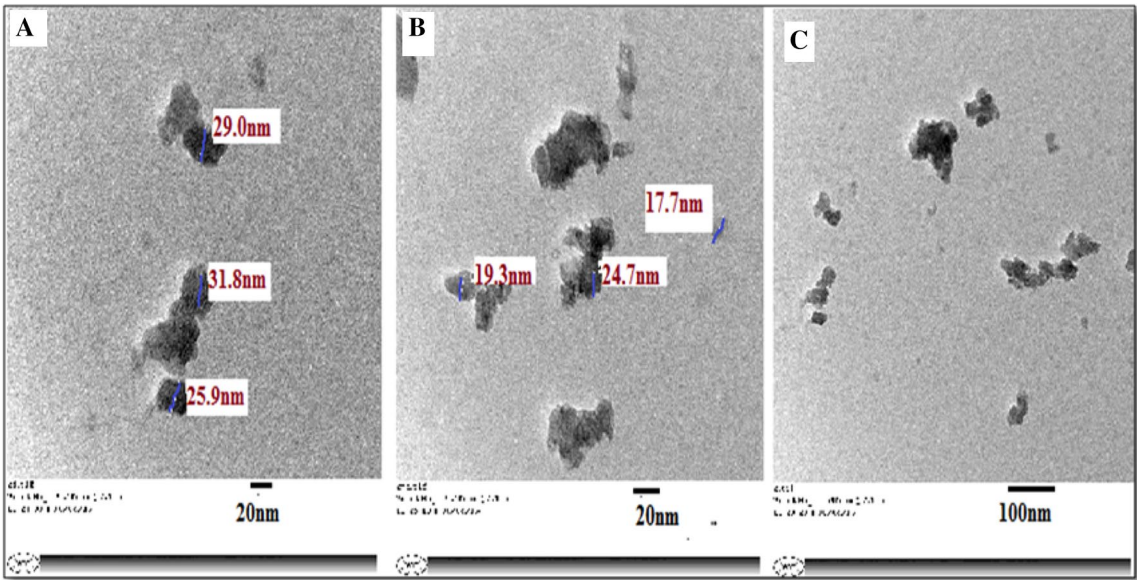

Fig. 4 TEM images of $SrMg_2Al_6Si_9O_{30}$ phosphor

be 20 nm. The crystallites are randomly distributed and looks like core structure as those reported in oxides based nanomaterials.

Here we have also estimated the crystallite from observed diffraction data by Debye Scherer's equation, which is comes out to be approximately 28 nm.

3.4 TGA

Thermal analysis is mostly carried out to investigate phase changes, decomposition, and loss of water or oxygen and to construct related phase diagrams. In thermogravimetry (TG), loss of crystallization water or volatiles such as oxygen and CO_2 is given away by a weight loss. In differential thermal analysis (DTA) a phase change is generally related with either absorption or evolution of heat. Usually in DTA, exothermic reactions give an increase in temperature, and endothermic reaction leads to a decrease in temperature [16]. The results from thermo gravimetric and differential thermal analyses are generally reported in the form of curves describing the mass lost and temperature difference respectively from the sample material against temperature. The temperatures at which the thermal processes start on and ended are graphically demonstrated as below.

The typical TG/DTA curves (green line/blue line) recorded for $SrMg_2Al_6Si_9O_{30}$ matrix in air environment have been depicted in the Fig. 5. Thermogravimetry (TG) and differential thermal analysis (DTA) curves of the $SrMg_2Al_6Si_9O_{30}$ phosphor were recorded in the temperature range 40–900 °C. It shows basically four mass loss steps in the temperature region of 40–900 °C about at 49.8, 389.7, 587.2 and 877.2 °C. The thermal decomposition temperature

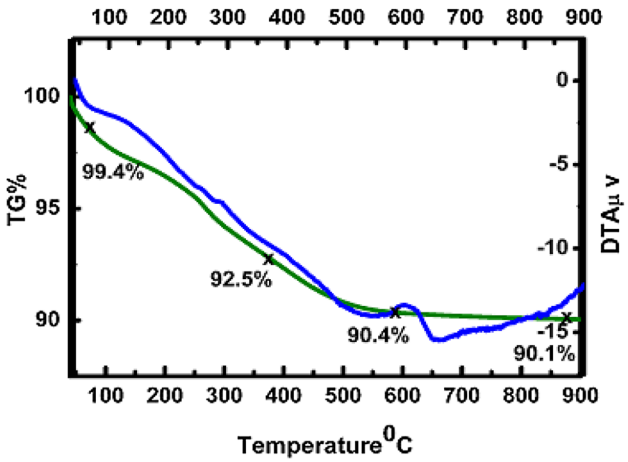

Fig. 5 TG/DTA curves of the $SrMg_2Al_6Si_9O_{30}$ phosphors

T_{dec} (The temperature when the sample loses 10% of its initial weight) is measured to be 587.2 °C The continuous nature of TG curve shows that there is no phase change during the rise of temperature up to 900 °C [17]. The TG curves show a sharp drop down up to 500 °C because of the weight loss of the sample due to elimination of water and the auto combustion reaction. This fall becomes lower between 500 and 600 °C and after 600 °C it remains constant with no significant weight loss. Due to the evaporation of water, there is weight loss below 500 °C. The DTA curve shows that the nanoparticles has curve below zero level meaning endothermic decrease Endothermic peaks at 90°, 550° are seen in the DTA curves which corresponds to the mass loss due to the release of H_2O in the TG curve while exothermic peak at

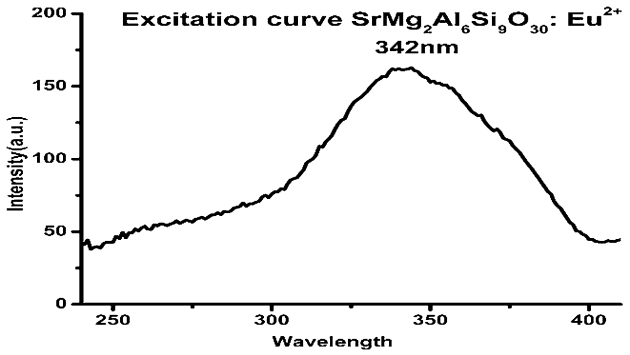

Fig. 6 Excitation curve of $SrMg_2Al_6Si_9O_{30}:Eu^{2+}$ phosphor ($\lambda_{em} = 425$ nm)

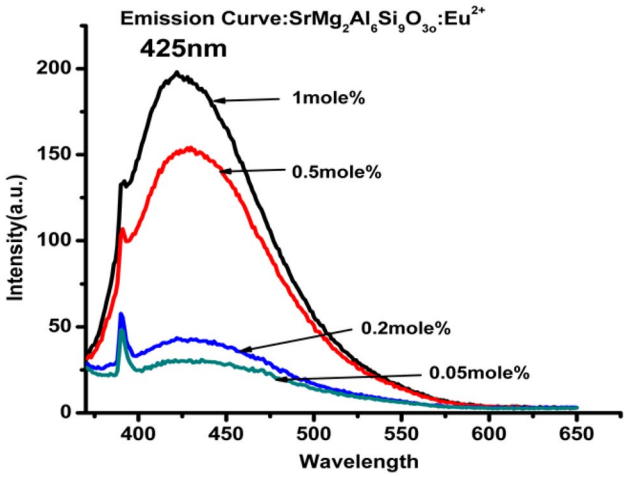

Fig. 7 Emission curve of $SrMg_2Al_6Si_9O_{30}:Eu^{2+}$ phosphor ($\lambda_{ex} = 342$ nm), where Eu^{2+} varies from 0.05 to 1 mol%

600 °C is attributable to the phase formation or crystallization of $SrMg_2Al_6Si_9O_{30}$ phases.

3.5 Luminescence

3.5.1 SMASO:Eu^{2+}phosphor

Figure 6 shows, the excitation spectra of the $SrMg_2Al_6Si_9O_{30}:Eu^{2+}$ phosphor recorded at $\lambda_{em} = 425$ nm. It shows a broad band from 220 to 400 nm. The band ranging from 220 to 300 nm is weaker as compared to that in the region from 300 to 400 nm. Application point of view this character of the phosphor is very useful. The excitation band centred at 342 nm is due to the $4f^7$–$4f^65d^1$ transition of Eu^{2+} ions. Monitored under the $\lambda_{ex} = 342$ nm, the emission spectra of the $SrMg_2Al_6Si_9O_{30}:Eu^{2+}$ is as shown in Fig. 7. It exhibits a broad emission band ranging from 380 to 550 nm with a shoulder around 390 nm which is the emission of the xenon lamp itself and an emission peak around 425 nm demonstrating blue luminescence, corresponding to the characteristic $4f^65d^1$–$4f^7$ transition of the Eu^{2+} ions. The particular emission of Eu^{3+} in the spectra is not visible demonstrating that the Eu^{3+} has been completely reduced to Eu^{2+}. It is seen that, the luminescence intensity increases gradually with the increase in the concentration of Eu^{2+} ions and becomes maximum at 1 mol%. The emission band appears to be almost symmetric indicating that Eu^{2+} ions occupy only one type (either of 12-fold coordinated Sr^{2+} site or six-fold coordinated Mg^{2+} site) of site in the $SrMg_2Al_6Si_9O_{30}$ matrix. The ionic radii of Eu^{2+} is 1.17 Å for CN = 6 and 1.26 Å for CN = 12, Mg^{2+} is 0.72 Å for CN = 6 and that of Sr^{2+} is 1.44 Å for CN = 12. Thus, it is closer to Sr^{2+} for 12 CN, hence Eu^{2+} will occupy Sr^{2+} site [11]. The chromaticity diagram is a tool to specify how the human eye will experience light with a given spectrum, which could naturally illumine the changes of the emission colour of the phosphor. Figure 8 shows the 1931 CIE chromaticity diagram for $SrMg_2Al_6Si_9O_{30}:Eu^{2+}$ phosphor at $\lambda_{ex} = 342$ nm for 1 mol% of Eu^{2+} concentration. The colour coordinates x = 0.160, y = 0.102 for the blue emitting $SrMg_2Al_6Si_9O_{30}:Eu^{2+}$ phosphor which may be a promising blue emitting phosphor for w-LEDs application.

3.5.2 SMASO:Ce^{3+} phosphor

The excitation spectrum of $SrMg_2Al_6Si_9O_{30}:Ce^{3+}$ phosphor monitored at $\lambda_{em} = 383$ nm is as shown in the Fig. 9 due to parity allowed 4f–5d transitions in Ce^{3+} ions. The energy of the electron in the 5d excited state is strongly influenced by the crystal field. Hence the 5d energy level splits into several energy sub-levels as shown in Fig. 10. The excitation spectrum is fitted well with five Gaussian broad bands peaking at 236, 249, 304, 318 and 324 nm. The Fig. 11, shows the emission spectrum of the $SrMg_2Al_6Si_9O_{30}:Ce^{3+}$ phosphor under the UV excitation of 321 nm from the xenon lamp. It shows a broad band with a peak at 383 nm. For $SrMg_2Al_6Si_9O_{30}:Ce^{3+}$ phosphor, Stokes shift of is found to be approximately equal to 5043 cm^{-1} which is in agreement to the values stated in the literature. As observed from Fig. 12, the emission spectrum observed in isolated broad band, hence it is well fitted with two emission centres peaking at 372 and 406 nm, respectively. The intensity of the band at 372 nm is remarkably higher than the one at 406 nm. Ce^{3+} has only one electron in the 4f shell. The ground state of Ce^{3+} is split into $^2F_{7/2}$ and $^2F_{5/2}$ (as shown in Fig.) with an energy difference of approximately 2200 cm^{-1} [18]. As shown in Fig. 13, the energy difference between $^2F_{7/2}$ and $^2F_{5/2}$ is found to be approximately 2251 cm^{-1}, which is in good agreement with the literature data. The asymmetric nature of the emission spectrum is consistent with prior research on the luminescence of Ce^{3+} in other hosts,

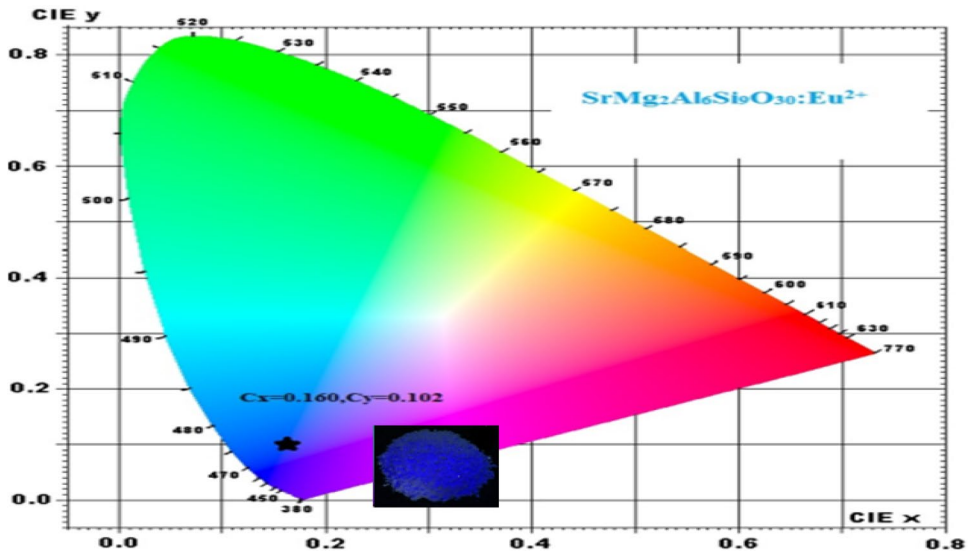

Fig. 8 CIE chromaticity diagram of $SrMg_2Al_6Si_9O_{30}:Eu^{2+}$phosphor

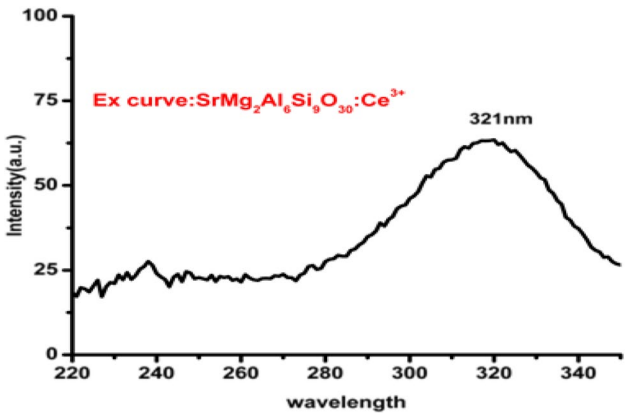

Fig. 9 PL excitation spectra of $SrMg_2Al_6Si_9O_{30}:Ce^{3+}$ phosphor ($\lambda_{em}=383$ nm)

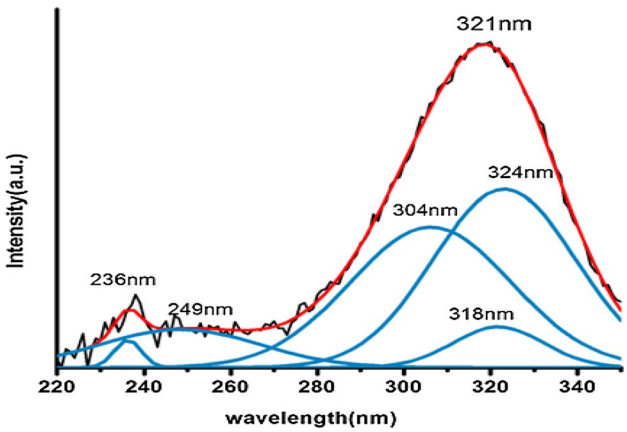

Fig. 10 Gaussian fit PLE spectra of $SrMg_2Al_6Si_9O_{30}:Ce^{3+}$ phosphor ($\lambda_{em}=383$ nm)

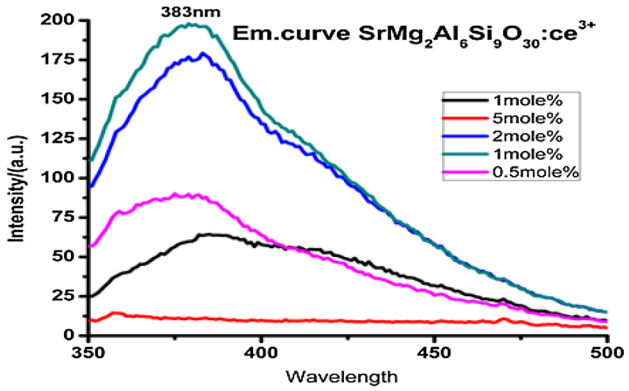

Fig. 11 PL emission spectra of $SrMg_2Al_6Si_9O_{30}:Ce^{3+}$ phosphor ($\lambda_{ex}=321$ nm)

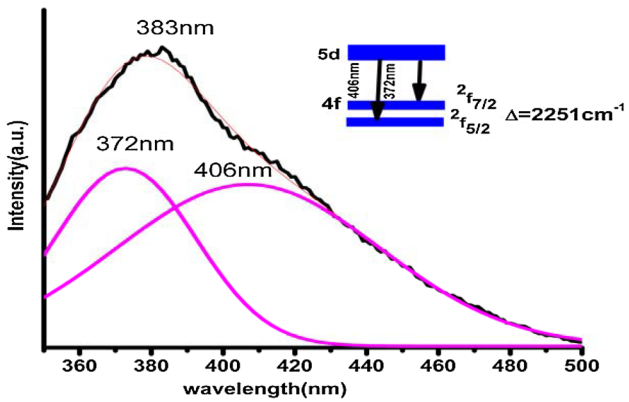

Fig. 12 Gaussian fit PL emission band of $SrMg_2Al_6Si_9O_{30}:Ce^{3+}$ phosphor

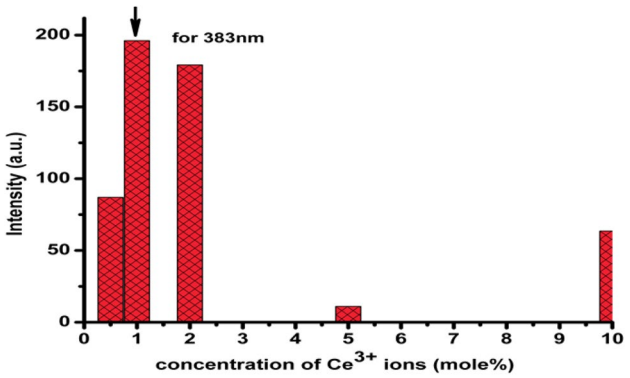

Fig. 13 Concentration quenching of $SrMg_2Al_6Si_9O_{30}:Ce^{3+}$ phosphor

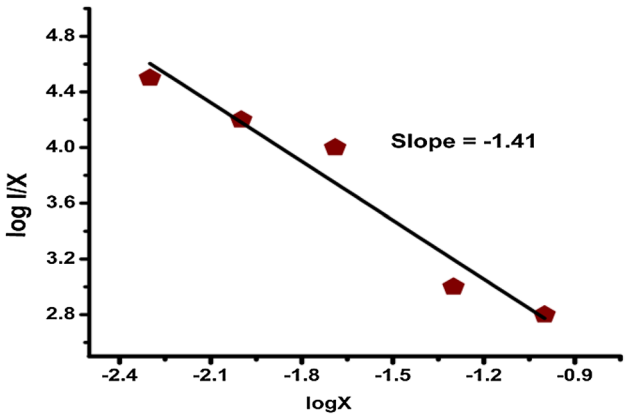

Fig. 14 The plot of log(I/x) versus log(x) $SrMg_2Al_6Si_9O_{30}:Ce^{3+}$ phosphors

such as $Y_3Al_5O_{12}$ (YAG) [19]. Figure 13 exhibits the emission spectra of $SrMg_2Al_6Si_9O_{30}:Ce^{3+}$ phosphor samples with different doping concentration. With the increase of Ce^{3+} ions concentration, the intensity of Ce^{3+} emission is increased initially till it reaches the maximum at 1 mol%, then gradually decreases due to the internal concentration quenching mechanism as shown in Fig. 14. In general, the concentration quenching mechanism is associated to energy transfer from one activator to another. The distance between the Ce^{3+} luminescent centers decreases with increase in the concentration of Ce^{3+} ions which marks more chance of nonradiative energy transfer between Ce^{3+} ions. The critical distance (R_C) for energy transfer between the Ce^{3+} ions [20], can be given by the equation:

$$R_C \approx 2\left(\frac{3V}{4\pi x_c N}\right)^{\frac{1}{3}} \quad (1)$$

where V represents the volume of the unit cell, x_c represents the critical concentration of the activator ions and N represents the number of cations in the unit cell. For $SrMg_2Al_6Si_9O_{30}:Ce^{3+}$ phosphor, parameters are $V = 1263.70$ Å^3, $N = 2$ and $x_c = 1$ Therefore, the R_C of $SrMg_2Al_6Si_9O_{30}:Ce^{3+}$ phosphor is estimated to be about 10.65 Å. As per Van Uitert [21] the energy transfer involves either multipolar interaction, radiation reabsorption or exchange interaction. As per Dexter [22] exchange interaction will come into play if the critical distance of energy transfer is < 5 Å. In $SrMg_2Al_6Si_9O_{30}:Ce^{3+}$ phosphor the R_c is found to be 10.65 Å > 5 Å, hence energy transfer by exchange interaction will not take place. If there exists considerable overlap between the luminescent spectra of the sensitizer and activator, radiation re absorption will come as outcome. There is no overlap between the excitation and emission spectra of $SrMg_2Al_6Si_9O_{30}:Ce^{3+}$ phosphor, hence no chance of energy transfer via radiation reabsorption. Thus, in $SrMg_2Al_6Si_9O_{30}:Ce^{3+}$ phosphor multipolar interaction is accountable for energy transfer. According to Van Uitert's [23, 24] the correlation between the luminescent intensity and their corresponding doping concentrations of the luminescent centre can be mathematically given by the following equation,

$$\frac{1}{x} = K\left[1 + \beta(x)\frac{\theta}{3}\right]^{-1} \quad (2)$$

where I is the emission intensity, x is critical concentration, K and b are constants, θ is a constant of the multipolar interaction between rare earth ions and equals to 6, 8 or 10 for electric dipole–dipole (d–d), electric dipole–quadrupole (d–q) or electric quadrupole – quadrupole (q–q) interactions, respectively. In order to calculate θ, log(I/x) versus log(x) is plotted, which results in a straight line with a slope equal to −θ/3. As shown in Fig. 11, the slope is −1.41 there by θ can be calculated as 4.23, which is close to 6. Thus, the quenching in $SrMg_2Al_6Si_9O_{30}:Ce^{3+}$ phosphor results from dipole–dipole interaction.

4 Summary

In the present work, Combustion synthesis technique has found to be successful methodology to synthesize a series of $SrMg_2Al_6Si_9O_{30}:Ce^{3+}$ and $SrMg_2Al_6Si_9O_{30}:Eu^{2+}$ nanophosphors at 600 °C. XRD pattern confirms the formation of pure phase at low temperature. Micro and nanoscale structure of phosphor is confirmed by SEM and TEM analysis the average crystallite size is found to be about 20 nm. TGA investigation shows the crystallization of $SrMg_2Al_6Si_9O_{30}$ phases at 600 °C. Optical properties of $SrMg_2Al_6Si_9O_{30}:Ce^{3+}$ phosphors show a broad emission band from 350 to 500 nm, centred at 383 nm under 321 nm excitation. The optimal concentration has found to be 1 mol%. The critical distance of energy transfer between Ce^{3+} ions has calculated

as 10.65 Å. The concentration quenching mechanism has been explained by the electric dipole interaction of the Ce^{3+} ions. Whereas Eu^{2+} emission in $SrMg_2Al_6Si_9O_{30}$ phosphor is observed at 425 nm under 342 nm excitation. The optimal concentration has found to be 1 mol%. Thus blue is an basic and most important colour component for the production of white light and there are only few rare earth available in periodic table that may gives an strong blue emission. Further, the $SrMg_2Al_6Si_9O_{30}:Eu^{2+}$ phosphor showed excellent CIE chromaticity co-ordinates (x = 0.160, y = 0.102) in the blue region, as a result it would be quite useful as a blue phosphor for SSL technology.

References

1. V.B. Pawade, A. Zanwar, R.P. Birmod, S.J. Dhoble, L.F. Koao, J. Mater. Sci. (2017). doi:10.1007/s10854-017-7536-8
2. Z.J. Zhang, A.C.A. Delsing, P.H.L. Notten, J.T. Zhao, H.T. Hintzen, Mater. Res. Bull. **47**, 2040 (2012)
3. R.C. Evans, L.D. Carlos, P. Douglas, J. Rocha, J. Mater. Chem. **18**, 1100 (2008)
4. C. Guo, H. Jing, T. Li, RSC Adv. **2**, 2119 (2012)
5. C.-H. Huang, P.-J. Wu, J.-F. Lee, T.-M. Chen, J. Mater. Chem. **21**, 10489 (2011)
6. B.N. Mahalley, S.J. Dhoble, R.B. Pode, G. Alexander, Appl. Phys. A **70**, 39 (2000)
7. P. Ghosh, A. Kar, A. Patra, Nanoscale **2**, 1196 (2010)
8. W. Lu, Y. Luo, Z. Hao, X. Zhang, X. Wang, J. Zhang, J. Lumin. **132**, 2439 (2012)
9. A. Kumar, S.J. Dhoble, D.R. Peshwe, J. Bhatt, J. Alloys Compd. **609**, 100 (2014)
10. A. Kumar, S.J. Dhoble, D.R. Peshwe, J. Bhatt, J. Alloys Compd. **578**, 389 (2013)
11. W. Lu, X. Zhanga, Y. Wang, Z. Hao, Y. Liu, Y. Luo, X. Wang, J. Zhang, J. Alloys Compd. **513**, 430 (2012)
12. W. Wolfgang, T. Armbruster, C. Lengauer, Eur. J. Mineral. **7**, 277 (1995)
13. W. Hou, Q. Wang, J. Colloid Interface Sci. **333**, 400 (2009)
14. W. Wang, T. Xue, Z.H. Jin, G. Qiao, J. Mater. Res. Bull. **43**, 939 (2008)
15. O. Silvestre, M.C. Pujol, F. Gueell, M. Aguilo, F. Diaz, A. Brenier, G. Boulon, Appl. Phys. B **87**, 111 (2007)
16. F. Zhang, T. Lan, W.J. Tang, Mater. Res. Bull. **64**,)128 (2015)
17. Z.W. Zhang, A.J. Song, X.H. Shen, Q. Lian, X.F. Zheng, Mater. Chem. Phys. **151**, 345 (2015)
18. M.Z. Hu, Y. Wu, H. Fu, C. Kang, J. Alloys Compd. **509**, 6476 (2011)
19. Z. Mu, Y. Hu, L. Chen, X. Wang, G. Ju, Radiat. Meas. **47**, 426 (2012)
20. G. Blasse, Phys. Lett. A **28**, 444 (1968)
21. L. Van Uitert, J. Electrochem. Soc. **114**, 1048 (1967)
22. D.L. Dexter, J. Chem. Phys. **21**, 836 (1953)
23. M. Kolte, V.B. Pawade, S.J. Dhoble, Appl. Phys. A **1**, 122 (2016)
24. V.B. Pawade, N.S. Dhoble, S.J. Dhoble, J. Rare Earths **593**, 32 (2014)